

## 4. INTERACTION REGION STRAIGHT

The interaction straight of eRHIC has to serve various purposes. First of all, it contains the actual interaction region where beams are colliding inside the eRHIC detector. While it is necessary to provide head-on collisions, beams must be separated as close as possible to the IP to allow low- $\beta$  magnets for both individual beams to be installed as close as possible to the IP without interfering with the other beam. Furthermore, since eRHIC is designed to collide longitudinally polarized beams, spin rotators are required to rotate the polarization direction of both beams from the vertical to the longitudinal direction. To measure the amount of resulting longitudinal polarization, polarimeters have to be embedded in the IR straight as well. The following sections present the IR design, the detector interface and the design of the spin rotators.

### 4.1 IR design

A preliminary design for the interaction region of the e-p collider eRHIC has been developed, which provides a luminosity of  $4.4 \cdot 10^{32} \text{ cm}^{-2} \text{ sec}^{-1}$  (see Table 1.1). This design has evolved from an earlier version [1] to provide sufficient space for focusing elements in both rings in spite of the fact that beam separation is less than some 20 cm. Figure 4.1 shows a 3D view of the interaction region.

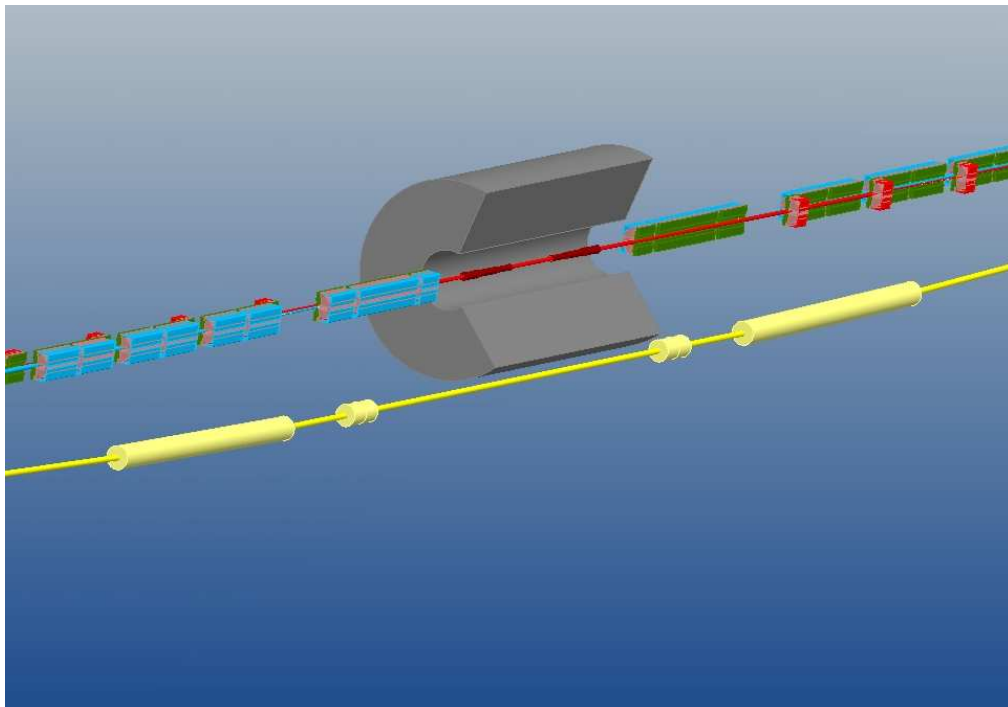


Figure 4.1: 3D view of the interaction region.

### 4.1.1 Electron IR Optics

Since electron  $\beta$  functions at the interaction point are almost equal,  $\beta_x = 0.19\text{ m}$ ,  $\beta_y = 0.27\text{ m}$ , focusing is provided by a superconducting quadrupole triplet inside the detector solenoid. With the horizontal emittance being about five times larger than the vertical one, the first and last magnet of that triplet are chosen to be focusing in the horizontal plane to keep the horizontal beam size small. The smaller vertical emittance in turn allows for a larger  $\beta$  function in the vertical plane, as it occurs inside the second, vertically focusing quadrupole. Figure 4.2 shows the quadrupole arrangement and  $\beta$  functions, while Table 4.1 lists some key parameters of the magnets.

With the first electron quadrupole, QE1, starting at a distance of 1.0 m from the interaction point, this configuration provides a free section of  $\pm 1.0\text{ m}$  around the IP to be used by detector components.

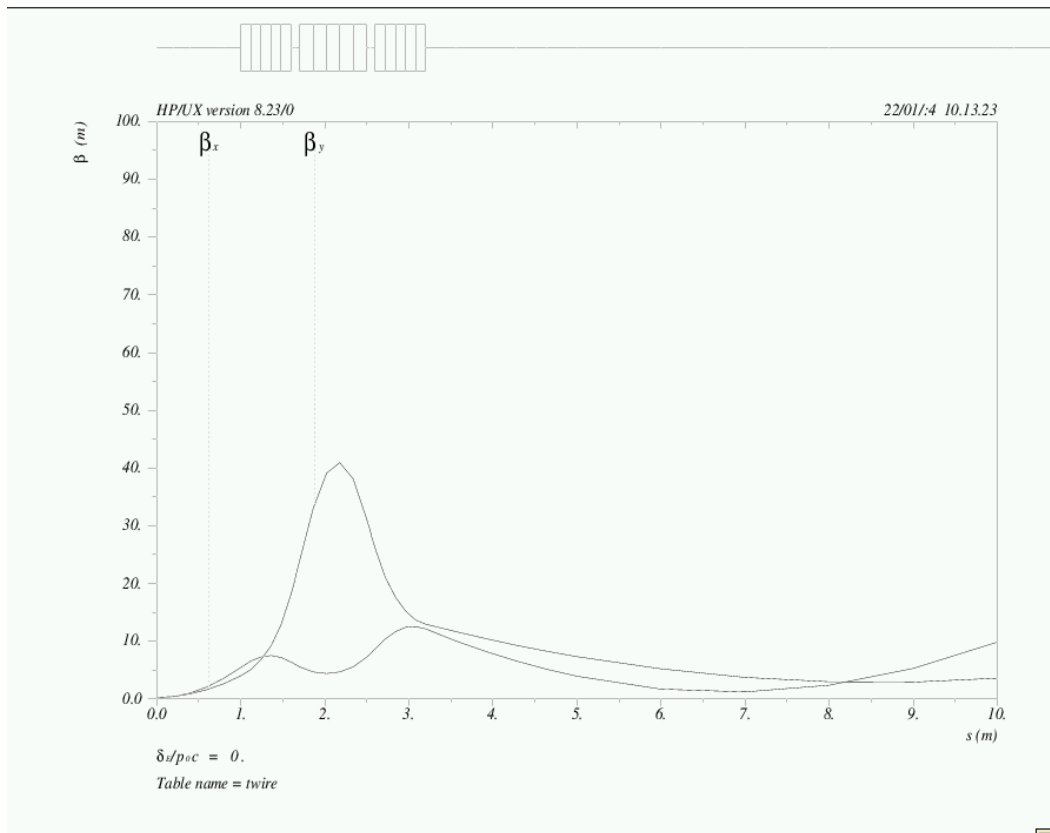


Figure 4.2: Electron IR lattice of the electron-ion collider eRHIC

The required minimum beam pipe radius is determined by the width of the synchrotron radiation fan that has to be passed safely through these magnets, as well as by the dimensions of the electron beam itself. For the latter, a minimum aperture of  $20\sigma_e$  has been used throughout the entire design of the interaction region, thus ensuring sufficient aperture even in the presence of orbit distortions.

Matching into the regular FODO lattice of the arcs is provided by septum quadrupoles which can be placed in-between the hadron low- $\beta$  quadrupoles, starting at a distance of 12.2 m from the IP.

Table 4.1: Magnet parameters for the electron triplets.

	QE1	QE2	QE3
length [m]	0.6	0.8	0.6
gradient [T/m]	83.3	76.7	56.7
radius [mm]	24	26	35
bending angle left/right [mrad]	2.50/-2.74	5.30/-2.02	0.0/-4.19
shift w.r.t. detector axis left/right [mm]	0/-10	0/-10	0/-10
tilt w.r.t. detector axis left/right [mrad]	1.25/-1.37	3.90/-2.38	3.90/-4.48
synchrotron radiation power left/right [W]	735/882	2475/360	0/2063
synchr. rad. power on septum left/right [W]	466/360	0/360	0/0
critical photon energy left/right [keV]	9.3/10.1	14.7/5.6	0/15.5

### 4.1.2 Hadron IR Optics

Hadron focussing is provided by a normal-conducting quadrupole doublet, starting 5m from the IP (Figure 4.3).

Septum quadrupoles are foreseen for both doublet lenses to keep the necessary separation between electron and hadron beam small, thus minimizing the width as well as the power of the resulting synchrotron radiation fan. Dedicated gaps in the hadron low- $\beta$  magnet string provide sufficient space for the septum quadrupoles in the electron ring.

Both lenses are split up into different individual magnets, with pole tip radii tailored according to the varying beam sizes. Pole tip fields are limited to 1.0 Tesla in all magnets to avoid saturation effects at the edges of the magnet poles. Table 4.2 lists the main parameters of these magnets.

Table 4.2. Parameter list of the hadron low- $\beta$  septum quadrupoles

	Q1	Q1B	Q1C	Q2	Q2B	Q2C	Q2D	Q2F	Q2G
length [m]	0.8	2.8	1.2	1.5	1.5	1.5	1.5	1.5	1.5
gradient [T/m]	58.3	41.7	33.3	20.2	17.0	16.2	16.2	16.2	17.0
pole tip radius [mm]	17.1	24.0	30.0	49.4	58.9	61.8	61.8	61.8	58.9
pole tip field [T]	1.0	1.0	1.0	1.0	1.0	1.0	1.0	1.0	1.0

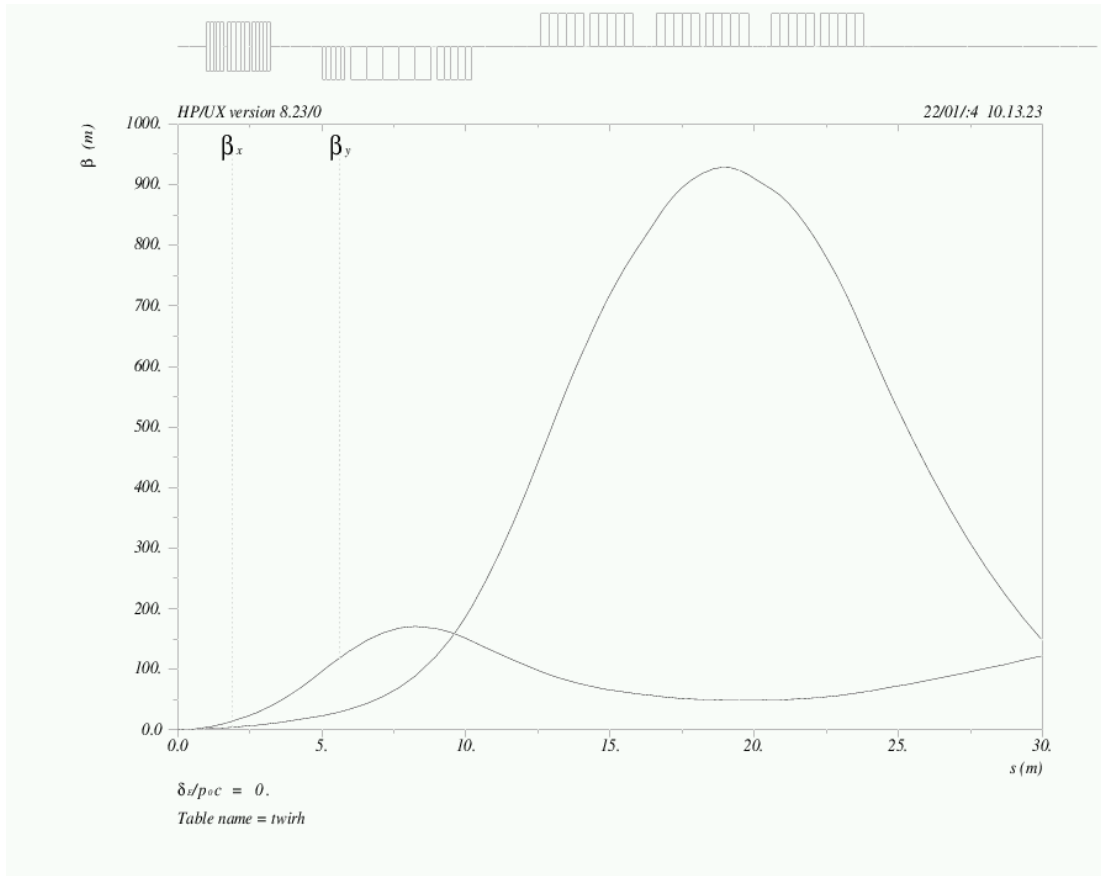


Figure 4.3: Hadron IR lattice of the electron-ion collider eRHIC.

### 4.1.3 Synchrotron Radiation Issues

The electron quadrupole triplet inside the detector volume is shared by the hadron beam. The focusing effect on the hadron beam is marginal due to the large energy difference - 10 GeV electrons compared to 250 GeV protons. This large energy difference in turn requires the beams to be separated such that the electrons do not experience the much stronger focusing fields of the hadron low- $\beta$  quadrupoles. This separation is provided by dipole windings in the superconducting electron low- $\beta$  quadrupoles. To minimize the necessary beam separation, the first hadron magnet is realized as a septum quadrupole, with a septum thickness of  $d_{\text{septum}} = 10$  mm, including beam pipes. Since the design apertures for the two beams are  $20\sigma_{x,e}$  for the electrons and  $12\sigma_{x,p}$  for the hadron beam, the required total separation between the orbits of the two beams at the location of the septum is therefore

$$\Delta x = 12\sigma_{x,p} + 20\sigma_{x,e} + d_{\text{septum}}. \quad (4.1)$$

Taking into account the  $\beta$  functions shown in Figure 4.2 and Figure 4.3, together with the respective emittances according to Table 1, the required beam separation is

$$\Delta x = 12 \cdot \sqrt{\beta_{x,p} \varepsilon_p} + 20 \cdot \sqrt{\beta_{x,e} \varepsilon_e} + d_{\text{septum}} = 12 \cdot 0.48 \text{ mm} + 20 \cdot 0.45 \text{ mm} + 10 \text{ mm} = 24.8 \text{ mm}. \quad (4.2)$$

When providing this separation using the dipole windings of the superconducting electron low- $\beta$  quadrupoles, this produces a synchrotron radiation fan that has to be passed safely through the detector beam pipe. Since some fraction of this synchrotron radiation fan unavoidably hits the septum on the electron downstream side (right side) of the detector, it was attempted to minimize the power and critical photon energy hitting the septum by distributing the bending angles in the individual dipole coils accordingly.

On the right side, this minimization is accomplished by a soft bend provided by the dipole coils in QE1 and QE2, which produce the part of the synchrotron radiation fan actually hitting the septum, and a strong bend in the QE3 that provides the required remaining separation angle to achieve sufficient separation at the septum.

This scheme cannot be adopted for the left side since a bend in the QE3 there would result in a very wide synchrotron radiation fan further downstream, where it would require large aperture magnets to be passed through. Since large aperture magnets would cover a significant fraction of the detector volume, this is therefore not desirable. Instead, a soft bend is provided by the QE1 alone, resulting in a synchrotron radiation fan that is just wide enough to cover the angle between the hadron beam orbit and the inner edge of the septum. The remaining beam separation is then provided by the QE2 dipole coil.

To further minimize the required magnet aperture, all quadrupoles on the right side are shifted towards the inside of the RHIC ring, resulting in an off-center electron orbit through these quadrupoles. The effect of this shift on the electron beam orbit is to be compensated by the dipole coils.

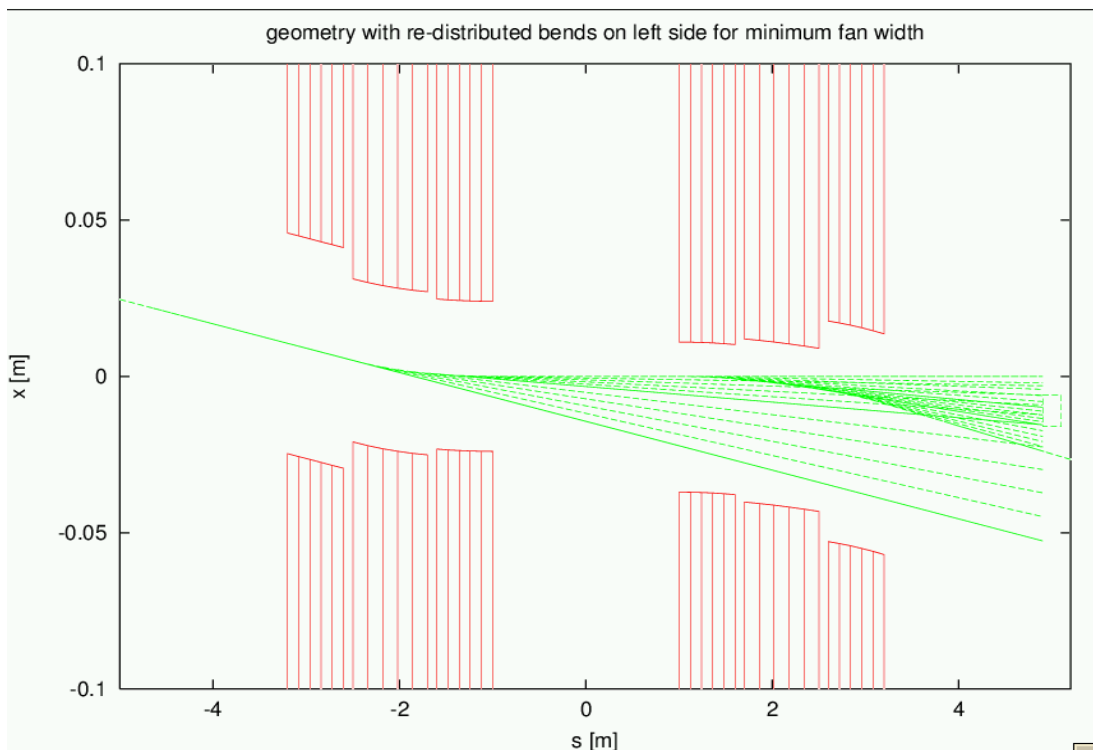


Figure 4.4: IR geometry and synchrotron radiation fan.

## 4.2 Hadron Insertion

A plan for the RHIC insertion is to remove the crossing dipoles at the eRHIC IP. This leads to the geometry shown in Figure 4.5 below:

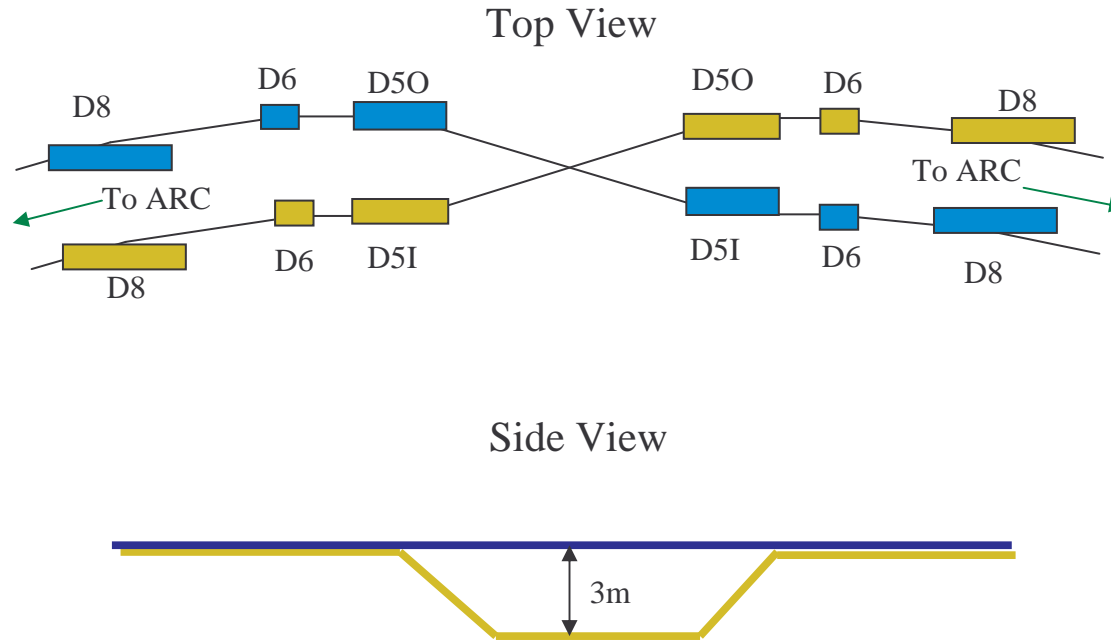


Figure 4.5: The top view and side view of the insertion. The electron beam collides with the Blue ring and the Yellow ring is moved out of the way.

Furthermore, the dipoles D50 are increased in bend angle by  $1.32\text{mrad}$  and D5I is decreased by  $1.32\text{mrad}$ . Both these changes will cause a path length change to the RHIC optics. We plan to change the horizontal bends, moving the beam line towards the center to adjust the path lengths.

For the Yellow ring, we will use a simple FODO cell design. The vertical bends will be placed such that the vertical dispersion is canceled. Additionally, there are no horizontal bends between the vertical bends so that the polarization is preserved. Figure 4.6 shows a design for the Yellow ring optics. The superconducting dipole bends are  $8.058\text{m}$  long with a  $32.22\text{mrad}$  bend angle. Thus, at  $B\rho = 831\text{Tm}$  the dipole field is  $3.43\text{T}$ , which is near the standard arc dipole of about  $3.6\text{T}$ . Furthermore, the length of this insertion is increased by  $15.8\text{cm}$  over the standard RHIC insertion.

The magnet parameters of the Yellow insertion are listed in Table 4.3

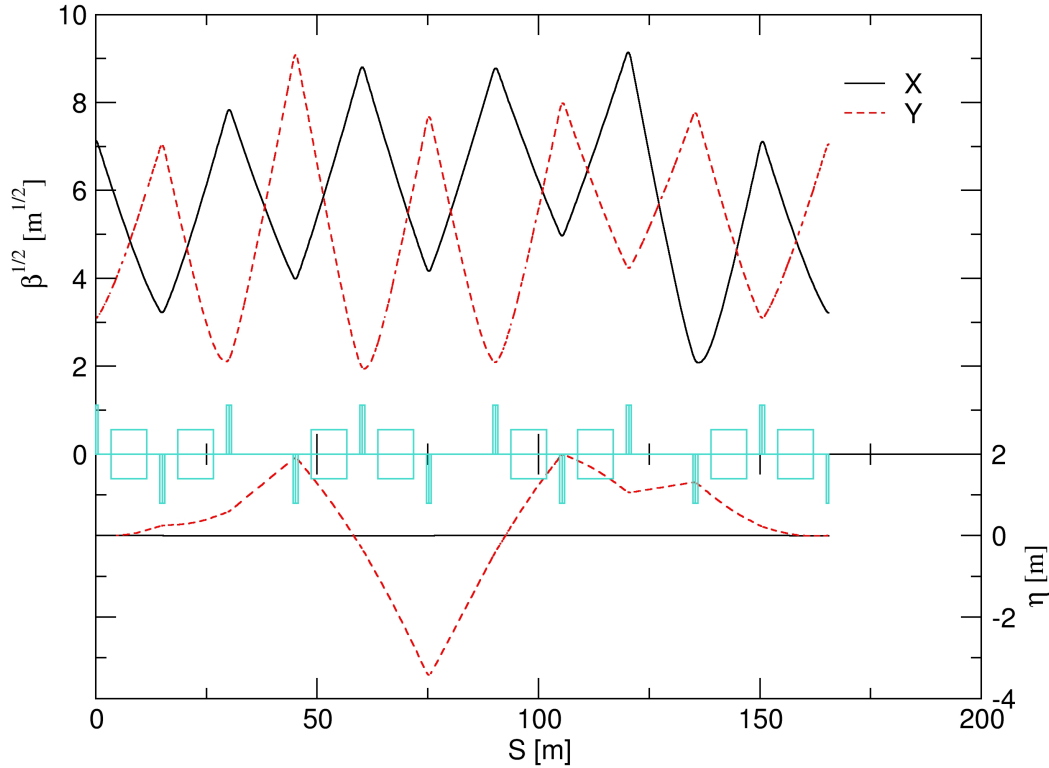


Figure 4.6: The insertion optics for the yellow ring. The fit was not perfect and there is a small residual vertical dispersion of about  $0.5\text{mm}$ . The trade off of larger beta functions, will allow the vertical dispersion matching to be further improved.

The electron beam will collide with the hadron beam in the blue ring. This insertion will produce a flat beam with  $\beta^*$ 's of  $(0.27, 1.08)\text{m}$  at the interaction point (IP). In order to produce a flat beam, a symmetric insertion design is used. Since, RHIC insertions are anti-symmetric, an additional half cell had to be added. This shifts the IP by about  $7.5\text{m}$  from original RHIC IP.

The triplet was designed to minimize the background from the electrons. This required using specialized quadrupoles with  $1\text{T}$  pole tip fields (non-superconducting). The strength is dependent on the allowable aperture. Furthermore, these triplet positions were adjusted so that they do not interfere with the electron ring magnets. This triplet design leads to  $\beta_{max}$  of  $1.4\text{km}$ .

The Blue ring IR insertion optics is shown in Figure 4.7. The magnet parameters of the Blue insertion are listed in Table 4.4

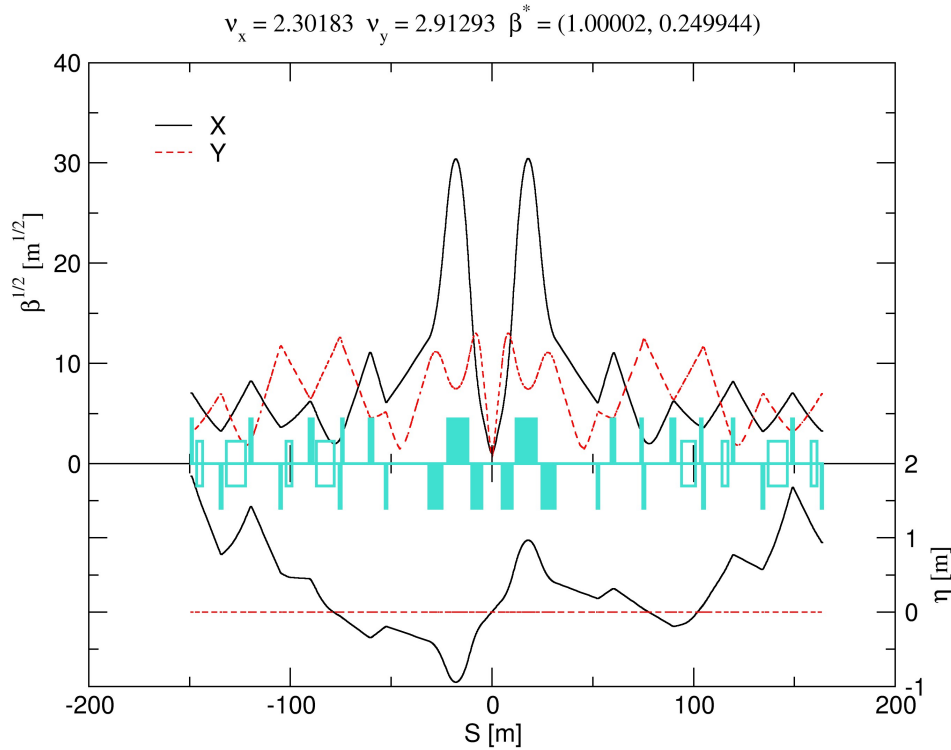


Figure 4.7: The insertion optics for the blue ring. This insertion is  $2.127\text{mm}$  shorter than the standard RHIC insertion. Note, the extra half cell on the right side, needed in order to convert this insertion to use symmetric optics.

### Alternative hadron insertion scheme

Here we describe an alternative approach<sup>3</sup> to the eRHIC insertion. In this case we remove the crossing dipoles for two insertions: 12 o'clock and 4 o'clock. Instead of having the connecting beam lines cross, they continue straight from blue to yellow at 12 o'clock and then return from yellow to blue at 4 o'clock, vice versa for the other ring. These two changes cancel leaving the other 4 insertions unchanged. Yellow ring does not need to make vertical excursion at this scheme and path lengths for Yellow and Blue ring circumferences are naturally equal. But there is a serious question as to whether breaking this symmetry will affect normal RHIC behavior. More studies are needed for this scheme.

<sup>3</sup> W. MacKay, private communication

Table 4.3. Yellow ring insertion magnet parameters.

<i>Device</i>	<i>Coil Radius [cm]</i>	<i>Length [m]</i>	<i>Field (250GeV protons) [T]</i>	<i>Gradient (250GeV protons) [T/m]</i>	<i>Drift space [m]</i>	
QF	4	1.110		67.59		2.941
V1	4	8.058	3.43		QF - V1	2.941
QD1	4	1.110		83.46	V1 - QD1	2.941
V1	4	8.058	3.43		QD1 - V1	2.941
QF1	4	1.110		62.90	V1 - QF1	2.941
QD2	4	1.110		88.17	QF1 - QD2	11.249
V2	4	8.058	3.43		QD2 - V2	2.941
QF2	4	1.110		59.74	V2 - QF2	2.941
V2	4	8.058	3.43		QF2 - V2	2.941
QD3	4	1.110		94.92	V2 - QD3	2.941
QF3	4	1.110		53.50	QD3 - QF3	11.249
V3	4	8.058	3.43		QF3 - V3	2.941
QD4	4	1.110		85.02	V3 - QD4	2.941
V3	4	8.058	3.43		QD4 - V3	2.941
QF4	4	1.110		68.56	V3 - QF4	2.941
QD5	4	1.110		61.77	QF4 - QD5	11.249
V4	4	8.058	3.43		QD5 - V4	2.941
QF5	4	1.110		82.65	V4 - QF5	2.941
V4	4	8.058	3.43		QF5 - V4	2.941
QD	4	1.110		69.76	V4 - QD	2.941

Table 4.4. Blue ring IR insertion magnet parameters. (Parameters of Q1,Q2 septum quadrupoles are listed in Table 4.2)

<i>Device</i>	<i>Name</i>	<i>Pole Tip or Coil Radius [cm]</i>	<i>Length [m]</i>	<i>Gradient (250GeV protons) [T/m]</i>	<i>Drift Space [m]</i>	
Q3	Q3a	5.98	1.5	16.72	Q2f - Q3a	2.745
	Q3b	5.98	1.5	16.72	Q3a - Q3b	0.200
	Q3c	5.98	1.5	16.72	Q3b - Q3c	0.200
	Q3d	5.98	1.5	16.72	Q3c - Q3d	0.200
Q4	Q4OT	4	0.75	66.52	Q3d - Q4OT	20.841
	Q4IT	4	0.75	66.52	Q3d - Q4IT	20.841
Q5	Q5Ob	4	1.11	75.08	Q5OTb - Q5Ob	0.131
	Q5OTb	4	0.75	32.85	Q4OT - Q5OTb	6.100
	Q5Ib	4	1.11	75.08	Q5ITb - Q5Ib	0.131
	Q5Ic	4	1.11	75.08	Q5ITc - Q5Ic	0.131
	Q5ITb	4	0.75	52.81	Q5Ic - Q5ITb	12.821
	Q5ITc	4	0.75	32.85	Q4IT - Q5ITc	6.100

## 4.3 Considerations on the Machine / Detector interface

### 4.3.1 Outline of the eRHIC Detector Design

The following discussion will be restricted to the nominal eRHIC collider mode operation of a 10GeV electron/positron beam colliding with a 250GeV proton beam. Simple four vector kinematics in e-p collisions which involves an electron and a proton in the initial state and a scattered electron along with a hadronic final state in the final state can be used to study analytically the energy and angular acceptance of the scattered electron and hadronic final state as a function of the main kinematic quantities in deep-inelastic scattering (DIS),  $x$  and  $Q^2$  [1]. This provides a first understanding of the final state topology.  $Q^2$  is the negative square of the momentum transfer between the incoming and scattered electron. The Bjorken scaling variable  $x$  is interpreted in the Quark-Parton model as the fraction of the proton momentum carried by the struck quark.

The hadronic final state consists of the current jet which emerges from the struck quark characterized by its polar angle and energy.

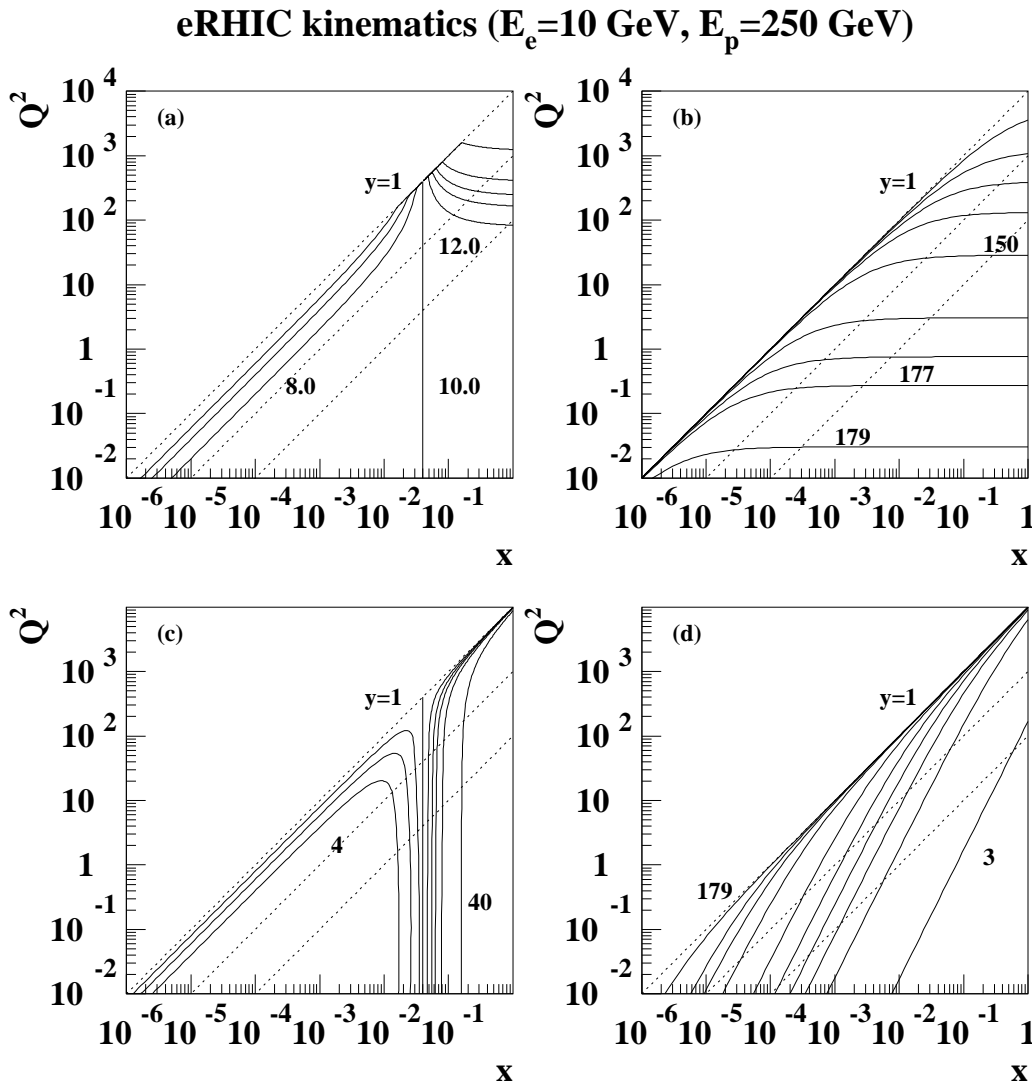


Figure 4.8: The dashed lines represent lines of constant  $y$  values (1, 0.1, 0.01). The electron beam energy amounts to 10GeV whereas the proton beam energy is 250GeV. Isolines of constant electron energies (4, 6, 8, 10, 12, 14, 16, 20 and 40GeV) (a), electron scattering angles ( $30^\circ$  -  $150^\circ$  in steps of  $30^\circ$  and  $170^\circ$ ,  $175^\circ$ ,  $177^\circ$  and  $179^\circ$ ) (b), current jet energies (4, 6, 8, 10, 12, 14, 16, 20 and 40GeV) (c) and current jet angles ( $3^\circ$ ,  $30^\circ$  -  $150^\circ$  in steps of  $30^\circ$  and  $170^\circ$ ,  $175^\circ$ ,  $177^\circ$  and  $179^\circ$ ) (d).

Figure 4.8 shows isolines of constant electron energy (a) and constant scattering angles (b) as well as lines of constant  $y$  values (1, 0.1, 0.01). The kinematic variable  $y$  is given in terms of  $x$  and  $Q^2$  ( $y = Q^2 / sx$ ) and refers to the inelasticity in the rest frame of the proton. The kinematic limit is given by  $y=1$ . The scattering angle is measured with respect to incoming proton beam which defines the positive  $z$  axis. Electron tagging acceptance down to at least  $177^\circ$  will be necessary to provide acceptance in  $Q^2$  below  $1\text{GeV}^2$ . The energy of the scattered electron is less than 10GeV and is in particularly small in the region of low  $x$  and medium to low values in  $Q^2$ . This sets stringent requirements on trigger and reconstruction efficiencies.

Figure 4.8 shows isolines of constant current jet energy (c) and angle (d). The energy of the current jet is rather small in the low  $x$  and medium to low  $Q^2$  region and overlaps to some extent with the scattered electron. The current jet energy increases towards the forward direction in the region of high  $x$  and  $Q^2$  values. This will require e/h separation capabilities in particular in the rear direction (incoming electron direction) and increasing jet energy measurement capabilities in the forward direction (incoming proton direction).

The following minimal requirements on a future eRHIC detector can be made:

- Measure precisely the energy and angle of the scattered electron (Kinematics of DIS reaction)
- Measure hadronic final state (Kinematics, jet studies, flavor tagging, fragmentation studies, particle ID)
- Missing  $E_T$  measurement for events involving neutrinos in the final state (Electroweak physics)

In addition to those demands on a central detector, the following forward and rear detector systems are crucial:

- Zero-degree photon detector to control radiative corrections, measure Bremsstrahlung photons for luminosity measurements and in e-A physics to tag nuclear de-excitation
- Tag electrons under small angles (Study of the non-perturbative/perturbative QCD transition region and luminosity measurement from Bremsstrahlung ep events)
- Tagging of forward particles (Diffraction and nuclear fragments)

Figure 4.9 show the first conceptual GEANT detector implementation of the above requirements on a central detector. The hermetic inner and outer tracking system is surrounded by an axial magnetic field on the order of 1-2T. The tracking volume is surrounded by a hermetic calorimeter system in the rear, barrel and forward direction. The calorimeter system is subdivided into electromagnetic and hadronic sections which are then in-turn subdivided into certain size towers. The inner most double functioning dipole and quadrupole magnets at a distance of 1m to the interaction region are also shown. The detailed design is under preparation.

The stringent requirements on the high-rate capability of the tracking system make a silicon-type detector for the inner tracking system (forward and rear silicon disks together with several silicon barrel layers) together with a GEM-type detector for the outer tracking system (forward and rear GEM-type tracking disks with several barrel GEM-type tracking layers) a natural choice.

The forward and rear detector systems have not been considered so far. The design and location of those detector systems has to be worked out in close collaboration to accelerator physicists since machine magnets will be employed as spectrometer magnets and thus determine the actual detector acceptance and ultimately the final location. It is understood that demands on optimizing the rear/forward detector acceptance might have consequences on the machine layout and is therefore an iterative process.

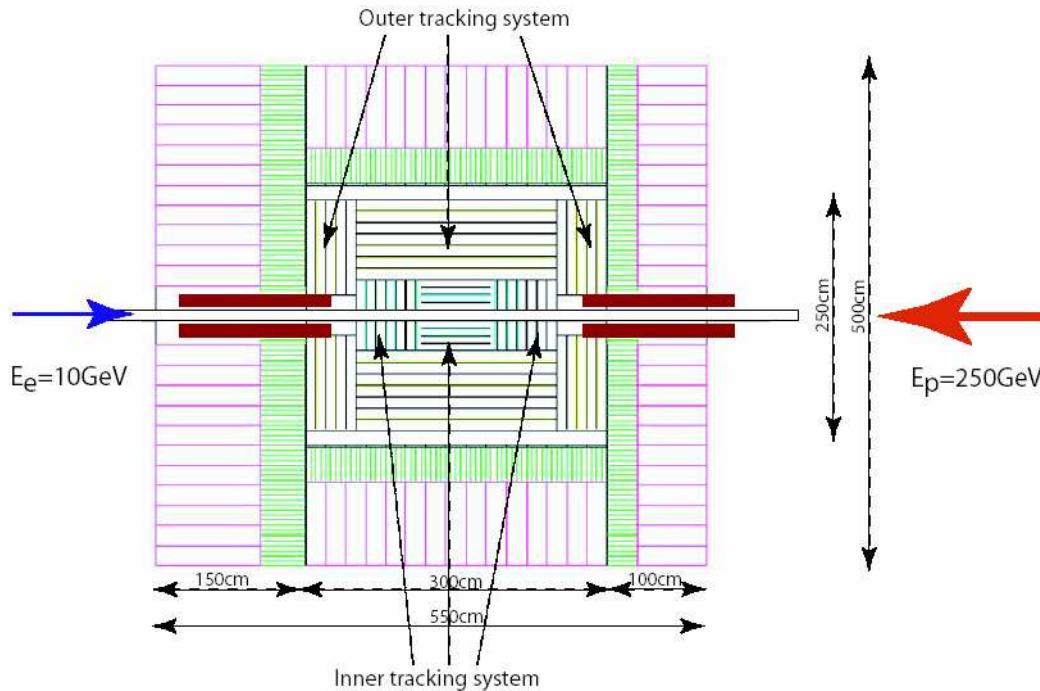


Figure 4.9: Conceptual GEANT detector implementation of the main central eRHIC detector components. The inner and outer hermetic tracking system is surrounded by an axial magnetic field on the order of 1-2T. The tracking volume is surrounded by a hermetic calorimeter system in the rear, barrel and forward direction.

### 4.3.2 Considerations on the Detector/Machine Interface

The following section provides an overview of some aspects on the detector/machine interface. The specification of those items has only recently been started.

- **Synchrotron radiation**

The location of the direct synchrotron radiation fan has been previously discussed. The direct synchrotron radiation has to pass through the entire interaction region before hitting a rear absorber system. This requires that the geometry of the beam pipe is designed appropriately with changing shape along the longitudinal beam direction which includes besides a simulation of the mechanical stress also the simulation of a cooling system of the inner beam pipe. The distribution of backscattered synchrotron radiation into the actual detector volume has to be carefully evaluated. An installation of a collimator system has to be worked. Those items have been started in close contact to previous experience at HERA.

- **Location of inner machine elements**

The demand of a high luminosity ep/eA collider facility requires the installation of focusing machine elements inside the actual detector volume. Such a scenario has been carried out as part of the HERA II luminosity upgrade with the installation of superconducting low beta quadrupole magnets. The inner most double functioning magnet as part of the electron lattice has an inner distance to the nominal interaction region of 80cm. Assuming an outer dimensions of 20cm in diameter, would restrict the  $Q^2$  acceptance to  $0.5\text{GeV}^2$ . A careful design of the inner tracking system to optimize the

tracking system is crucial. The optimization in acceptance will require a close collaboration between the actual detector design and the location of inner most machine elements which includes also the design of the inner beam pipe. The GEANT simulation on those aspects has been started. A first conceptual implementation is shown in Figure 4.9.

- **Rear electron tagging system**

The need for acceptance of scattered electrons below the central detector acceptance is driven by the need for luminosity measurement through e-p/e-A Bremsstrahlung and photo-production physics. Besides that a calorimeter setup to tag radiated photons from initial-state radiation and Bremsstrahlung will be necessary. The scattered electrons will pass through the machine elements and leave the pipe through special exit windows. The simulation of various small-angle calorimeters has only been started. This will require a close collaboration with the eRHIC machine design efforts to aim for an optimal detector setup.

- **Forward tagging system**

The forward tagging system beyond the central detector will play a crucial role in diffractive ep/eA physics and in eA physics in general. A significant fraction of the hadronic final state is produced in the forward direction.

The design of a forward tagger system based on forward calorimetry and Roman pot station is foreseen. Charged particles will be deflected by forward machine elements. This effort will require as well a close collaboration with the eRHIC machine design efforts to ensure the best possible forward detector acceptance.

## 4.4 Electron Spin Rotator Design

A spin rotation from vertical direction in the arcs to longitudinal one in the IPs will be performed in two steps: at first, by a solenoidal spin rotator to horizontal plane and then by dipoles. The  $\pm 90^\circ$  spin rotator consists of two superconducting solenoids, each 3 m long, and with the field of 8.7 T. Between solenoids is placed a focusing structure, which cancels the betatron coupling and also creates the spin transparency. On the opposite side of the interaction straight, spin is restored to vertical direction by the negative spin rotator. As a result, the spin tune is undisturbed by the interaction region insertion, and the polarization behavior is mainly the same as without the spin rotators.

The equilibrium polarization direction (vector  $\mathbf{n}_0$ ) is vertical in the main part of the ring and therefore one can expect a relatively low depolarization rate of the electron beam. Moreover, the Sokolov-Ternov polarization mechanism should provide a high enough beam polarization.

Still there are some requirements, which should be satisfied by the insertion optics, where the spin vector  $\mathbf{n}_0$  lies in the horizontal plane. To minimize the negative effect from a spin perturbation  $\mathbf{w}$  over the whole straight section, we should fulfill the so called spin transparency condition, namely, the integral of the perturbation through the insertion azimuth  $\theta$ :

$$I = \int_{\theta_1}^{\theta_2} \mathbf{w} \cdot \boldsymbol{\eta} d\theta$$

should be made zero or, at least, small. Here  $\boldsymbol{\eta} = \boldsymbol{\eta}_1 - i\boldsymbol{\eta}_2$  is a complex vector, which is composed from the unity vectors  $\boldsymbol{\eta}_1$  and  $\boldsymbol{\eta}_2$ , which in turn are the two orthogonal solutions of the spin motion equation for the equilibrium particle. The spin perturbation components are:

$$w_x = \nu_0 z'' + K_x \frac{\Delta\gamma}{\gamma}$$

$$w_z = -\nu_0 x'' + K_z \frac{\Delta\gamma}{\gamma}$$

$$w_y = K_y \frac{\Delta\gamma}{\gamma}$$

where  $\nu_0 = \gamma a$  is the dimensionless spin tune,  $z''$  and  $x''$  are the second derivatives of the vertical or horizontal displacements over the azimuth  $\theta$ ,  $K_{x,y,z}$  are respectively the normalized horizontal, longitudinal or vertical magnetic fields.

Careful analysis shows that the spin transparency condition for the interaction region straight section, which contains the discussed above spin rotators, can be fulfilled, and a small decrease of the equilibrium polarization degree is caused only by bending magnets in the straight between two spin rotators.

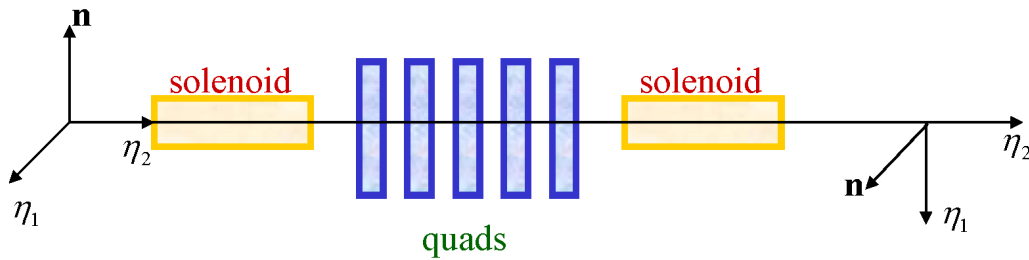


Figure 4.10: Scheme of the solenoidal spin rotator in the electron ring.

The scheme of the focusing structure has been found (see Figure 4.10), that contains only regular quadrupoles inside the solenoidal spin rotator and cancels the betatron coupling as well as creates the spin transparency. Transfer matrices of a full insertion (from the first solenoid edge to the second solenoid edge):

$$T_x = \begin{pmatrix} 0 & -2r \\ (2r)^{-1} & 0 \end{pmatrix}, \quad T_z = \begin{pmatrix} 0 & 2r \\ -(2r)^{-1} & 0 \end{pmatrix}$$

Here  $r$  is a curvature radius in the solenoidal field  $B_y$ :

$$r = B\rho/B_y$$

Table 4.5. Main parameters of the rotator insertion.

Parameter	Value
Solenoid length	3 m
Solenoidal field	8.7 T
Quadrupole length	0.4 m
Maximal quad's gradient	28 T/m

In proposed design the condition on transparency is fulfilled, thus, all spin rotators as well as the horizontal wiggle between them are spin transparent against the betatron motion deviations. An inevitable spin-orbit coupling for the energy-off particles is excited by the first spin rotator and then compensated by the second one. In result the spin-orbit coupling vector  $\mathbf{d} = \gamma \frac{\partial \mathbf{n}}{\partial \gamma}$  is exactly equal to zero in arcs (see Figure 4.11).

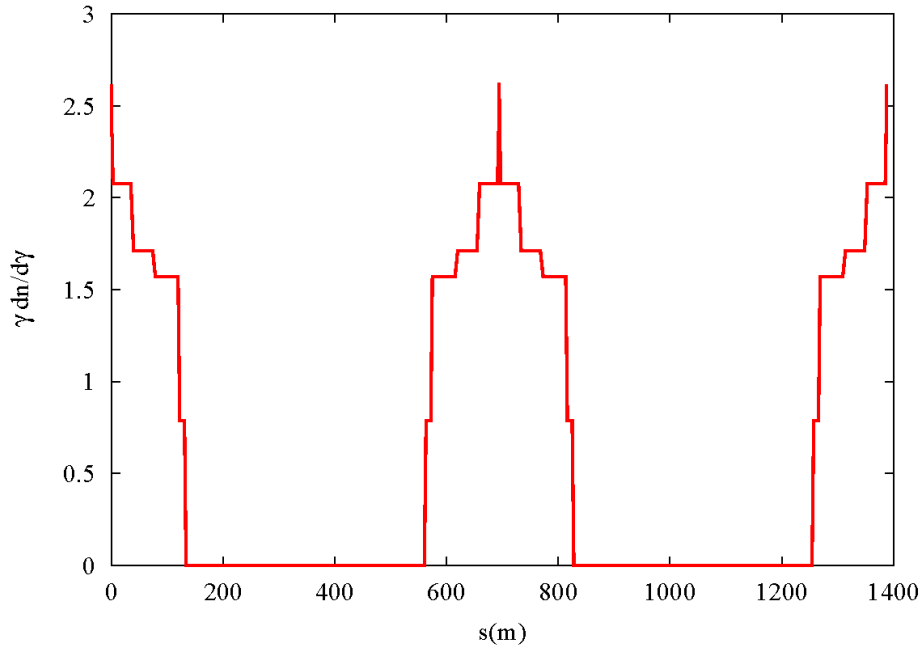


Figure 4.11: Spin-orbit coupling along the ring.

## References:

- 1 C. Montag et al., Proceedings of the 30th Advanced ICFA Beam Dynamics Workshop on High Luminosity e+e- Collisions, Stanford, (2003)
- 2 B. Surrow, 'Measurement of the Proton Structure Function F2 at Low Q2 and Very Low x with the ZEUS Beam Pipe Calorimeter at HERA', *EPJdirect* **C2** (1999)

